Biochemical Characterization and Crystal Structure Determination of Human Heart Short Chain L-3-Hydroxyacyl-CoA Dehydrogenase Provide Insights into Catalytic Mechanism†

Joseph J. Barycki,‡ Laurie K. O'Brien,§ Judy M. Bratt,‡ Rongguang Zhang,|| Ruslan Sanishvili,|| Arnold W. Strauss,§ and Leonard J. Banaszak*,‡

Department of Biochemistry, Molecular Biology, and Biophysics, University of Minnesota, Minneapolis, Minnesota 55455, Department of Pediatrics, School of Medicine, Washington University, St. Louis, Missouri 63110, Structure Biology Center, Center for Mechanistic Biology and Biotechnology, Argonne National Laboratory, Argonne, Illinois 60439

Received December 9, 1998; Revised Manuscript Received March 1, 1999

ABSTRACT: Human heart short chain L-3-hydroxyacyl-CoA dehydrogenase (SCHAD) catalyzes the oxidation of the hydroxyl group of L-3-hydroxyacyl-CoA to a keto group, concomitant with the reduction of NAD^+ to NADH, as part of the β-oxidation pathway. The homodimeric enzyme has been overexpressed in *Escherichia coli*, purified to homogeneity, and studied using biochemical and crystallographic techniques. The dissociation constants of NAD^+ and NADH have been determined over a broad pH range and indicate that SCHAD binds reduced cofactor preferentially. Examination of apparent catalytic constants reveals that SCHAD displays optimal enzymatic activity near neutral pH, with catalytic efficiency diminishing rapidly toward pH extremes. The crystal structure of SCHAD complexed with NAD^+ has been solved using multiwavelength anomalous diffraction techniques and a selenomethionine-substituted analogue of the enzyme. The subunit structure is comprised of two domains. The first domain is similar to other α/β dinucleotide folds but includes an unusual helix-turn-helix motif which extends from the central β-sheet. The second, or C-terminal, domain is primarily α-helical and mediates subunit dimerization and, presumably, L-3-hydroxyacyl-CoA binding. Molecular modeling studies in which L-3-hydroxybutyryl-CoA was docked into the enzyme−NAD^+ complex suggest that His 158 serves as a general base, abstracting a proton from the 3-OH group of the substrate. Furthermore, the ability of His 158 to perform such a function may be enhanced by an electrostatic interaction with Glu 170, consistent with previous biochemical observations. These studies provide further understanding of the molecular basis of several inherited metabolic disease states correlated with L-3-hydroxyacyl-CoA dehydrogenase deficiencies.

The metabolism of fatty acids by β-oxidation is a primary source of energy for several tissues including heart, muscle, and liver. Each cycle of β-oxidation shortens the saturated acyl-CoA by two carbons with the release of acetyl-CoA. Four mitochondrial enzymes are involved in this cycle: acyl-CoA dehydrogenase, 2-enoyl-CoA hydratase, L-3-hydroxyacyl-CoA dehydrogenase, and 3-ketoacyl-CoA thiolase. L-3-Hydroxyacyl-CoA dehydrogenase [EC 1.1.1.35] catalyzes the oxidation of the hydroxyl group of L-3-hydroxyacyl-CoA to a keto group, concomitant with the reduction of NAD^+ to NADH, as shown below.

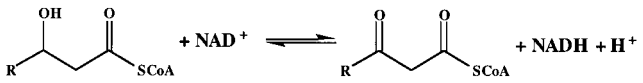

The enzyme is a "B-side"-specific dehydrogenase (*1*) with hydride transfer occurring on the *si* face of the nicotinamide ring. L-3-Hydroxyacyl-CoA dehydrogenases bear a consensus gly-x-gly-x-x-gly motif, suggesting the presence of a signature α/β nucleotide-binding fold, and a histidine residue has been localized to the enzyme active site (*2*, *3*).

L-3-Hydroxyacyl-CoA dehydrogenases have been isolated from the mitochondria of several species (*4*, *5*), as well as from peroxisomes (*6*, *7*). In addition, it has been reported that a λ-crystallin, a major rabbit lens protein, is in fact an L-3-hydroxyacyl-CoA dehydrogenase (*8*). Presumably due to the varying chain lengths of fatty acids that necessarily pass through the β-oxidation pathway, distinct isoforms of these enzymes with differing, but overlapping, chain-length specificities have evolved. In general, two forms of L-3-hydroxyacyl-CoA dehydrogenase are encountered. Short chain L-3-hydroxyacyl-CoA dehydrogenase (SCHAD)[1] is a soluble dimeric enzyme with a subunit molecular weight of approximately 34 kDa, which displays optimal activity using 6-carbon substrates (*9*). In addition to the short chain

† The project is supported by a NIH postdoctoral fellowship grant to J.J.B. (1F32-DK09759-01) and research support to L.J.B. from the NIH (GM13925). Use of the Argonne National Laboratory Structural Biology Center beamline at the Advanced Photon Source was supported by the U.S. Department of Energy, Office of Energy Research, under Contract No. W-31-109-ENG-38.

* To whom correspondence should be addressed: Dr. Leonard J. Banaszak, Dietrich Professor of Biochemistry, Department of Biochemistry, Molecular Biology, and Biophysics, 4-225 Millard Hall, 435 Delaware Street S.E., Minneapolis, MN 55455. Phone: (612) 626-6597. Fax: (612) 624-5121. E-mail: len_b@dcmir.med.umn.edu.

‡ University of Minnesota.

§ Washington University.

|| Argonne National Laboratory.

10.1021/bi9829027 CCC: $18.00
Published on Web 04/14/1999

metabolizing enzyme, a long chain specific form of L-3-hydroxyacyl-CoA dehydrogenase, LCHAD, has also been identified. LCHAD is a part of a membrane-associated multifunctional protein and exhibits optimal activity toward substrates containing 12−16 carbons in the acyl chain. SCHAD and LCHAD share considerable sequence homology and display overlapping substrate specificity (*10*). Recently, a potential third member of the L-3-hydroxyacyl-CoA dehydrogenase enzyme family has been reported, which also catalyzes the oxidation of short chain L-3-hydroxyacyl-CoA substrates but shares no significant sequence homology to SCHAD or LCHAD (*11*).

Numerous inherited disorders of fatty acid oxidation have been described, including deficiencies of SCHAD and LCHAD activities (*9*). Most often these deficiencies are manifested as hypertrophic cardiomyopathy, skeletal myopathy, hypoketotic hypoglycemia, and liver dysfunction (*12*−*14*). Recently, LCHAD deficiency within the α-subunit of human mitochondrial trifunctional protein has been correlated with maternal acute fatty liver of pregnancy (AFLP), sudden unexplained infant death, and Reye-like syndrome (*14*). Thus, considerable interest has arisen in the characterization of this family of enzymes. Since human SCHAD is a soluble mitochondrial matrix protein, it is much more amenable to study than LCHAD, a component of a membrane-associated multifunctional enzyme complex.

In a previous report from this laboratory, a preliminary α-carbon chain tracing of pig heart short chain L-3-hydroxyacyl-CoA dehydrogenase complexed with NAD^+ was described, in which the double-domain structure of the enzyme was depicted (*15*). Binding of the NAD^+ cofactor occurred in the amino-terminal domain, which displayed some structural homology to other dinucleotide-binding domains. The second or carboxy-terminal domain appeared to be exclusively α-helical and was thought to be involved in acyl-CoA substrate binding as well as subunit dimerization. However, the pig heart model could not be sufficiently refined to include amino acid side chain positions because of the peculiar occurrence of three subunits within the asymmetric unit. A complete dimer was found within the asymmetric unit, and a second dimer was centered about a crystallographic 2-fold axis. In addition, due to poor electron density in the carboxy-terminal domain, inaccuracies in the α-carbon trace of this region were suspected (Dr. L. J. Banaszak, unpublished observation).

In this report, the biochemical characterization and structure determination of human heart SCHAD are described. Enzyme dissociation constants for reduced and oxidized cofactor were determined over a broad pH range, as were apparent kinetic constants for the conversion of acetoacetyl-CoA to L-3-hydroxybutyryl-CoA. The crystal structure of SCHAD[2] was obtained by multiple wavelength anomalous diffraction (MAD) techniques using selenomethionine-substituted SCHAD. These studies provide insight into the catalytic mechanism of the enzyme, identify amino acid residues important in substrate recognition, and provide a greater understanding of the molecular basis of SCHAD and LCHAD deficiencies.

MATERIALS AND METHODS

Expression and Purification of L-3-Hydroxyacyl-CoA Dehydrogenase. The cDNA encoding human heart L-3-hydroxyacyl-CoA dehydrogenase has been isolated and subcloned for overexpression in *Escherichia coli* (*2*, *16*). To facilitate subsequent purification, a pET21a vector was chosen to express the enzyme with a C-terminal hexameric histidine tag (rSCHADH6).[3] The recombinant construct was used to transform *Escherichia coli* strain BLR (DE3). Cultures, grown to an OD_{600} of 0.6−1.0 in LB media at 37 °C, were induced overnight by the addition of isopropyl thio-β-D-galactoside (IPTG) to a final concentration of 2 mM. The cells were harvested by centrifugation and resuspended in 0.1 M sodium phosphate buffer, pH 7.8, containing 0.3 M NaCl. Cells were lysed by sonication and centrifuged. The supernatant was then treated with 0.35% polyethylenimine at 4 °C and centrifuged to separate precipitated nucleic acids from the protein-containing supernatant. The enzyme was purified by affinity chromatography using a nickel-chelating column (Novagen) following the manufacturer's protocol. The enzyme was then dialyzed against 50 mM potassium phosphate buffer, pH = 7.2, containing 1 mM dithiothreitol (DTT).

Selenomethionine-substituted enzyme (SeMET-rSCHADH6) was prepared by expression of the same plasmid construct in a methionine-requiring auxotroph strain of *Escherichia coli*, B834(DE3). The bacteria were grown at 37 °C to an OD_{600} of 1.0−1.5 in M9 minimal media containing 0.4% glucose. The medium was supplemented with 19 amino acids (-Met) and selenomethionine at 40 μg/mL, as well as with the vitamins riboflavin, niacinamide, pyridoxine monohydrochloride, and thiamine, each at 1 mg/mL, following the protocol described by Ramakrishnan *et al.* (*17*). Cells were induced with 2.0 mM IPTG overnight and harvested. Purification of SeMET-rSCHADH6 was performed as described above, but included the addition of 10 mM DTT to the enzyme solution immediately after elution from the nickel-chelating column, as well as to the dialysis buffer, to prevent oxidation of the selenomethionine. To confirm incorporation of eight selenomethionine residues per enzyme monomer, enzyme samples were dialyzed against 50 mM ammonium acetate buffer, pH = 8.0, and analyzed by electrospray mass spectrometry by the Analytical Chemistry and Biomarkers Core at the University of Minnesota Cancer Center.

Dissociation Constant Determination. Dissociation constants for NAD^+ and NADH were determined by fluores-

[1] Abbreviations: AFLP, acute fatty liver of pregnancy; CNS, Crystallography and NMR System; DTT, dithiothreitol; FOM, figure of merit; IPTG, isopropyl thio-β-D-galactoside; LCHAD, long chain L-3-hydroxyacyl-CoA dehydrogenase; MAD, multiple wavelength anomalous diffraction; 6PGDH, 6-phosphogluconate dehydrogenase; rSCHADH6, recombinant human short chain L-3-hydroxyacyl-CoA dehydrogenase containing a C-terminal hexameric histidine tail; SCHAD, short chain L-3-hydroxyacyl-CoA dehydrogenase; SeMet-rSCHADH6, selenomethionine-substituted rSCHADH6.

[2] Coordinates and structure factors for rSCHADH6 and its selenomethionine-substituted analogue have been deposited in the Protein Data Bank with accession codes 3HAD and 2HDH, respectively.

[3] After this manuscript was submitted and accepted for publication, a spurious mutation was found within the current plasmid encoding rSCHADH6 which results in substitution of Phe 80 with a cysteine residue. The F80C mutation is surface-exposed and located in the middle of α-helix 3. It is not within the cofactor or acyl-CoA substrate binding site and does not appear to alter the catalytic activity or structural integrity of the protein.

Table 1: Dissociation Constants of Nicotinamide Cofactors As Determined by Fluorescence Titration of Human rSCHADH6[a]

pH	K_d (μM) NAD^+	K_d (μM) NADH
5.0	109.1 ± 8.6	0.34 ± 0.02
6.0	143.0 ± 13.8	0.48 ± 0.04
7.0	85.8 ± 21.1	0.73 ± 0.04
8.0	34.2 ± 4.2	0.93 ± 0.08
9.0	7.3 ± 0.7	3.81 ± 0.22
10.0	21.7 ± 1.7	>30[b]

[a] Buffers used in the determinations are 0.1 M citrate/phosphate (pH 4−6), 0.1 M potassium phosphate (pH 6−8), and 0.1 M bis-tris propane (pH 8−10). [b] The quenching end point was uncertain and therefore the indicated value is an approximation.

Table 2: Apparent Steady State Kinetic Constants of Acetoacetyl-CoA Reduction by Human Heart rSCHADH6[a]

pH	K_m (μM acetoacetyl-CoA)	V_{max} (μmol substrate/min/mg enzyme)	k_{cat} (s^{-1})	k_{cat}/K_m ($\mu M^{-1}\ s^{-1}$)
5.0	34.5 ± 7.7	281 ± 19.0	155	4.5
6.0	45.0 ± 2.3	448 ± 7.6	246	5.5
7.0	18.7 ± 2.2	459 ± 19.0	252	13.5
8.0	13.8 ± 1.6	205 ± 11.4	113	8.2

[a] Measurements were made at a [NADH] of 100 μM, a saturating concentration as judged by observed dissociation constants (Table 1) and previously reported K_m values of related L-3-hydroxyacyl-CoA dehydrogenases (*3*, *6*).

cence quenching experiments (*6*). Measurements were made at excitation and emission wavelengths of 285 and 335 nm, respectively, over the pH range of 5.0−10.0. Buffers used for characterization included 0.1 M citrate/phosphate (pH 4−6), 0.1 M potassium phosphate (pH 6−8), and 0.1 M bis-tris propane (pH 8−10). rSCHADH6 was titrated with increasing amounts of cofactor and the resulting decrease in protein fluorescence intensity monitored. The dissociation constant was calculated from the concentration of cofactor that results in half-maximal decrease in fluorescence intensity.

Kinetic Characterization of rSCHADH6. Enzyme activity was measured by monitoring the conversion of acetoacetyl-CoA to L-3-hydroxybutyryl CoA and the concomitant oxidation of NADH to NAD^+. The reaction was monitored at 340 nm following the decrease in absorbance of NADH as described in Noyes and Bradshaw (*4*). For standard screening of enzyme activity during purification, the enzyme assay was performed in 0.1 M sodium phosphate buffer, pH 6.3, containing 0.1 mM dithiothreitol, 0.1% Triton-X 100, 30 mM NADH, and 40 mM acetoacetyl-CoA. To ascertain the apparent kinetic constants of the enzymatic conversion of acetoacetyl-CoA to L-3-hydroxybutyryl-CoA, including K_m, V_{max}, and k_{cat} values, rSCHADH6 activity was assayed at several pH values (see above) in the presence of 100 μM NADH, a saturating concentration as judged by examination of dissociation constants (Table 1), and varying concentrations of acetoacetyl-CoA.

Crystallization of SCHAD. Crystals of human heart short chain L-3-hydroxyacyl CoA dehydrogenase were grown in the presence of 5 mM NAD^+ by the hanging drop method out of a solution of 50 mM *N*-[2-acetamido]-2-iminodiacetic acid, pH 6.5, within the precipitant range of 14−19% polyethylene glycol 4000 at a protein concentration of 5 mg/mL. To collect data at cryogenic temperatures, crystals were transferred to artificial mother liquor containing cryoprotectant. This was accomplished in a stepwise fashion by soaking the crystals, for a duration of 1−2 min, in artificial mother liquor containing increasing amounts of glycerol (5% increments) until a final glycerol concentration of 20% was attained (*18*).

X-ray Diffraction Studies. Multiwavelength anomalous diffraction studies (*19*) using SeMET-rSCHADH6 enzyme crystals complexed with NAD^+ were conducted under cryogenic conditions on Beamline 19-ID of the Structural Biology Center−CAT at Argonne National Laboratory's Advanced Photon Source. The selenium absorption spectrum was measured as X-ray fluorescence using a Bicron scintillation counter. Four wavelengths were selected for data collection corresponding to the inflection point (0.9794 Å), the peak (0.9792 Å), and two remote energies (0.9355 Å, 1.078 Å) with respect to the absorption edge of selenium. Complete data sets were collected successively for each wavelength from the unoriented crystal on the SBC APS1 3 × 3 CCD area detector. Each data set required approximately 12 min to collect (58 frames, 2° each, 10 s/frame). A high-resolution native data set was also collected of rSCHADH6 complexed with NAD^+. Intensities were integrated using DENZO and scaled with SCALEPACK (*20*).

Structure Determination. Phases were calculated using the program SOLVE, version 1.02, utilizing Bayesian-correlated MAD phasing techniques (*21*). Data collected at the absorption peak (λ_3) were treated as the reference data set and resolution limits of 8.0 to 2.5 Å were imposed. Theoretical values of f' and f'' were used and allowed to refine during analysis. The resulting values are nearly identical to the theoretical values and are given in Table 3. Although a dimer was predicted within the asymmetric unit, a self-rotation function revealed no definitive axis of noncrystallographic symmetry. Therefore, noncrystallographic symmetry constraints could not be employed within the peak search program used for the structure determination. The resulting phase information produced a readily interpretable electron density map, which was subjected to solvent flattening and histogram mapping using the program DM within the CCP4 program suite.

Model Building and Refinement. An initial model of SeMET-rSCHADH6 was constructed using the program, MAID (*22*), in which greater than 90% of the amino acids were assigned based on the initial electron density map. The model was refined using Crystallography and NMR System (CNS) (*23*), with a bulk solvent correction and a refinement target of "maximum likelihood based on amplitudes" employed throughout refinement; noncrystallographic symmetry constraints were not used. The initial rounds of model refinement included torsional dynamics, simulated annealing, positional refinement, and B-factor refinement using the data collected at λ_3 from 10 to 2.5 Å. Subsequent rounds instead utilized reflections from 20 to 2.2 Å using data collected at λ_1 in which Bijvoet pairs had been merged (Table 3). The program O was used for model rebuilding after each round of refinement (*24*).

The coordinates for NAD^+ were obtained from the Heterocompound Information Centre−Uppsala (HIC−Up), and the ligand was added to each subunit once the R_{cryst} value dropped below 25.0%. Also at this point, water molecules obeying proper hydrogen-bonding constraints with electron

Table 3: Data Collection Statistics

data set	λ_1 (1.0781 Å)	λ_2 (0.9794 Å)	λ_3 (0.9792 Å)	λ_4 (0.9355 Å)	λ_1 (bijvoets merged)	rSCHADH6
source of data[a]	19-ID	19-ID	19-ID	19-ID	19-ID	19-ID
space group	$P2_12_12_1$	$P2_12_12_1$	$P2_12_12_1$	$P2_12_12_1$	$P2_12_12_1$	$P2_12_12_1$
cell dimensions						
a (Å)	50.65	50.59	50.62	50.60	50.65	50.23
b (Å)	86.50	86.42	86.46	86.45	86.50	86.02
c (Å)	169.18	169.09	169.13	169.14	169.18	167.81
resolution (Å)	20−2.5	20−2.5	20−2.5	20−2.5	20−2.2	40−2.0
% complete	98.1	97.9	98.0	97.3	90.2	99.2
% highest shell	97.0	98.4	98.2	97.7	60.3	99.5
no. of reflections	25 841	25 711	25 773	25 664	34 779	48 014
redundancy	4.6	4.6	4.6	4.6	1.8	3.5
$I/\sigma I$	8.9	8.5	8.0	8.8	10.4	7.6
R_{sym} (%)[b]	5.6	7.8	7.9	6.8	3.5	5.8
f'	−3.48	−10.0	−7.94	−4.37		
f''	0.49	4.63	3.85	2.64		

[a] 19-ID corresponds to data collected at the 19-ID undulator beamline of the Structural Biology Center. [b] $R_{sym} = \sum (|I - \langle I \rangle|)/\sum I$.

densities greater than 1.0 σ on a $2|F_o| - |F_c|$ map and 4.0 σ on an $|F_o| - |F_c|$ map were included. Furthermore, as the quality of the maps improved, residues were added to the N-terminal and C-terminal ends of the peptide chains. An additional model of rSCHADH6 complexed with NAD^+ was constructed based on the refined SeMET-rSCHADH6 model with refinement proceeding as above. Coordinates are deposited in the PDB with the accession codes 2HDH and 3HAD for the SeMET-rSCHADH6 and rSCHADH6 models, respectively.

Molecular Modeling Studies. Molecular modeling studies were conducted within the DOCKING module of InsightII software package (Molecular Simulations, Inc.). Coordinates for acetoacetyl-CoA were obtained from the recently solved structure of rat liver mitochondrial enoyl-CoA hydratase complexed with acetoacetyl-CoA (PDB entry 1DUB) (*25*). The 3-keto group of the CoA compound was converted to the corresponding hydroxyl group using the BUILDER module. rSCHADH6 displays considerable structural homology to 6-phosphogluconate dehydrogenase (6PGDH) whose structure has been determined with its substrate, 6-phosphogluconate (*26*). Therefore, L-3-hydroxybutyryl-CoA was placed initially by superposition of equivalent atoms in 6-phosphogluconate. Docking studies sought to minimize steric overlaps and maximize electrostatic interactions between L-3-hydroxybutyryl-CoA and rSCHADH6. In addition, the C3 of L-3-hydroxybutyryl-CoA was required to be within 3 Å of C4 of the nicotinamide ring of NAD^+, and similarly, the 3-OH group of the substrate within 3 Å of Nϵ2 of His 158.

RESULTS

Protein Expression, Purification, and Characterization. rSCHADH6 and SeMET-rSCHADH6 have been expressed in *Escherichia coli* and purified to homogeneity by affinity chromatography. Modest expression levels of rSCHADH6 are observed (∼3−4 mg/L of culture), which are greatly reduced within the selenomethionine expression system used to obtain SeMET-rSCHADH6 (∼0.5 mg/L of culture). Nonetheless, sufficient amounts of enzyme were readily obtained. A single affinity chromatography step, using a nickel-chelating resin, produced enzyme that was >98% pure as judged by SDS−PAGE (data not shown). Incorporation of eight selenomethionine residues into SeMET-rSCHADH6 was confirmed by electrospray mass spectrometry. rSCHADH6 exhibits a molecular weight of 33846.7 ± 2.6 Da in close agreement with a calculated mass of 33813.7 Da for mature SCHAD containing an additional N-formyl initiator methionine and six-histidine carboxy-terminal tail. SeMET-rSCHADH6 has an observed mass of 34252.2 ± 4.4 Da, comparable to a calculated mass of 34188.9 Da for rSCHADH6 containing selenium instead of sulfur within each of its eight methionine residues. The observed mass differences, approximately 33 Da for rSCHADH6 and 63 Da for SeMET-rSCHADH6, are probably the result of oxidation since DTT could not be included in the sample dialysis buffer used in preparation for electrospray mass spectrometry analysis.

Determination of dissociation constants for nicotinamide cofactors and kinetic characterization of rSCHADH6 were conducted. The dissociation constants of NAD^+ and NADH were determined by measuring quenching of tryptophan fluorescence in rSCHADH6 upon addition of nicotinamide cofactor. The results, shown in Table 1, reveal that rSCHADH6 binds NADH more tightly than NAD^+ by an order of magnitude or greater in the neutral pH range. Generally, the affinity of the enzyme for NAD^+ increases with increasing pH; a corresponding decrease in affinity for NADH with increasing pH is also observed. However, this trend does not hold at very basic pH (pH > 9). rSCHADH6 exhibits a specific activity of approximately 200 μmol of substrate/min/mg of enzyme, when assayed under standard conditions (see Materials and Methods), with SeMET-rSCHADH6 displaying a similar level of activity (data not shown). The kinetic data, summarized in Table 2, indicate that rSCHADH6 exhibits optimal activity for the conversion of acetoacetyl-CoA to L-3-hydroxybutyryl-CoA in the neutral pH range, with catalytic activity diminishing sharply toward extremes of pH.

Crystallization and X-ray Diffraction Studies. Crystals of rSCHADH6 and SeMET-rSCHADH6 suitable for X-ray diffraction studies were grown by the hanging drop method out of a solution of 50 mM *N*-[2-acetamido]-2-iminodiacetic acid, pH 6.5, with polyethylene glycol 4000 as the precipitant. Typically, crystals grown in the presence of 5 mM NAD^+ attained dimensions of 0.1 mm × 0.1 mm × 0.3 mm within 3 to 5 days at 18 °C. X-ray diffraction data were collected under cryogenic conditions from crystals of

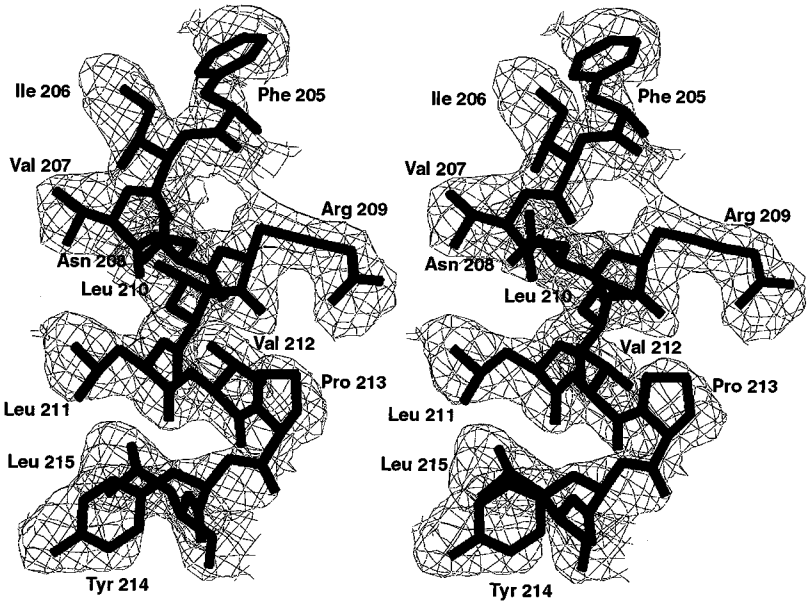

FIGURE 1: Representative MAD-phased electron density. The stereo drawing depicts residues 205−215 of the final rSCHADH6 model superimposed on the corresponding experimentally derived electron density, which is contoured at 1σ.

rSCHADH6 and SeMET-rSCHADH6, each complexed with NAD^+. The results are summarized in Table 3. The crystals belong to space group $P2_12_12_1$ with a Matthews coefficient, V_m, of 2.7 Å^3/Da, based on the assignment of two monomers within the asymmetric unit. However, a self-rotation function revealed no definitive dyad axis.

MAD data were collected as part of the commissioning testing of Beamline 19-ID of the Structural Biology Center−CAT at Argonne National Laboratory's Advanced Photon Source. In contrast to more traditional approaches, complete data sets were collected at successive wavelengths from the unoriented crystal, with no evidence of significant crystal decay (Table 3, $\lambda_1-\lambda_4$). The SeMET-rSCHADH6 crystals diffracted to 2.2 Å with low R_{sym} values. A native data set of rSCHADH6 complexed with NAD^+ was also obtained which included data to 2.0 Å resolution (Table 3, rSCHADH6).

Structure Determination and Model Refinement. MAD phasing techniques were used in the structure determination of SeMET-rSCHADH6. By examining anomalous and dispersive differences, 14 selenium positions (out of a possible 16) were identified with the two unidentified sites corresponding to the initiator methionine residue of each subunit which is disordered in the final model. The positions of the selenium atoms were used to generate phase information, which resulted in a readily interpretable electron density map and an initial figure of merit (FOM) of 0.61. Solvent flattening and histogram mapping provided only modest improvements in the quality of the electron density map (FOM = 0.63). After subsequent determination of the noncrystallographic symmetry operator, noncrystallographic averaging was attempted; the resulting map provided no advantage and was not used. In particular, the averaging degraded the electron density of numerous amino acid side chains throughout the protein. This degradation was most evident in the helix-turn-helix tail of the NAD^+-binding domain (α2, α3) and the loop regions of the C-terminal α-helical domain. Not surprisingly, these regions correspond to areas of relatively greater rms differences between the two subunits of the dimer. The degradation observed upon ncs-averaging further illustrates the excellent quality of the initial phase information.

Table 4: Model and Refinement Statistics

	SeMET-rSCHADH6	rSCHADH6
resolution (Å)	20−2.2	40−2.0
σ cutoff	0.0	0.0
no. of reflections	32 575	45 242
R_{cryst} (%)[a]	19.8	21.8
R_{free} (%)[b]	25.1	26.4
no. of protein atoms	4482	4482
no. of ligand atoms	88	88
no. of water molecules	254	320
average B-factor (Å^2)	40.2	47.4
rmsd bond lengths (Å)	0.007	0.008
rmsd bond angles (deg)	1.3	1.4
rmsd dihedral (deg)	20.4	20.4
rmsd improper (deg)	0.71	0.78
Ramachandran geometry[c]		
most favored (%)	88.8	89.5
allowed (%)	10.9	9.9
generously allowed (%)	0.4	0.6
disallowed	−	−
cis-peptides	2	2

[a] $R_{cryst} = \Sigma|F_o - F_c|/\Sigma|F_o|$. [b] An R_{free} test set of 5% of the total reflections was used. [c] The Ramachandran geometry was monitored using PROCHECK (*27*).

A representative region of the experimentally derived MAD-phased electron density map is depicted in Figure 1. Amino acid residues 205−215 from the final SMET-rSCHADH6 model are superimposed on the density. Greater than 90% of the amino acid residues of SeMET-rSCHADH6 were built into the experimentally derived electron density map prior to refinement using CNS. Positive electron density for NAD^+ and numerous ordered water molecules was observed within the MAD-phased electron density map, but these elements were not added until later rounds of refinement when the R_{cryst} value dropped below 25%. Additional residues were also added as the quality of the maps improved. Final statistics of the SeMET-rSCHADH6 enzyme structure are summarized in Table 4.

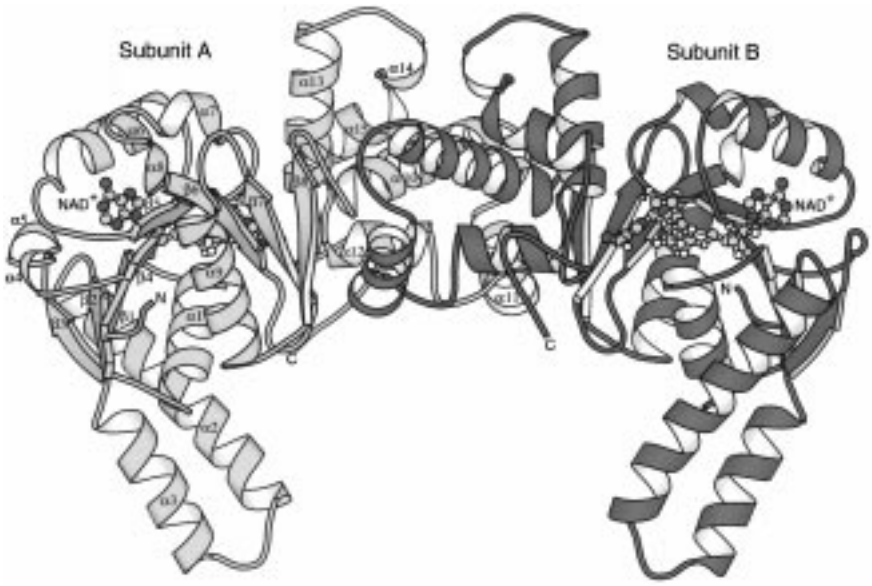

FIGURE 2: Ribbon diagram illustrating the final model of the rSCHADH6 dimer complexed with NAD^+. Subunit A is depicted in light gray and subunit B in dark gray, with N- and C-termini and secondary structure elements indicated. NAD^+ is shown as a ball-and-stick representation bound to each subunit.

A model of rSCHADH6 complexed with NAD^+ was constructed based upon the refined SeMET-rSCHADH6 model and required only a few rounds of refinement. The SeMET-rSCHADH6 and the rSCHADH6 models are nearly identical with a root-mean-square (rms) deviation of 0.30 Å for α-carbon atoms and 0.51 Å for all atoms. These values are comparable to the rms deviation between equivalent atom positions within the rSCHADH6 dimer of 0.51 Å for α-carbon atoms and 0.81 Å for all atoms. The SeMET-rSCHADH6 and rSCHADH6 models are of nearly equal quality with the SeMET-rSCHADH6 model having slightly lower R_{cryst} and R_{free} values (Table 4). Examination of the two structures revealed that substitution with selenomethionine did not significantly perturb the structure of the enzyme, and therefore, further discussion will be limited to the rSCHADH6 model, unless otherwise noted.

Overall Structure. The final model of rSCHADH6 with bound cofactor is pictured in Figure 2. The N- and C-termini are labeled, and subunits of the dimeric model with their respective NAD^+ cofactor are indicated. Note that due to poor electron density the first 12 residues and the majority of the C-terminal hexameric histidine tag are not included in the model. rSCHADH6 exhibits a two-domain topology, with the N-terminal domain of the monomer (residues 12−201) having a β-α-β fold similar to $NAD(P)^+$-binding enzymes. It consists of a core eight-stranded β-sheet flanked by α-helices. The first six strands of the sheet are in a parallel conformation as observed in a typical Rossmann fold. The final two strands are also parallel but run in the opposite direction relative to the first six strands. An interesting feature of the N-terminal domain is the large helix-turn-helix "tail" which connects strands 2 and 3 of the central β-sheet. This motif extends from the NAD^+-binding domain and contains numerous charged amino acid side chains. The amino acid sequence in this fingerlike protrusion is apparent in the α2 and α3 regions as given in Figure 3.

The C-terminal domain (residues 207−302) consists primarily of α-helices and is involved in subunit dimerization and, presumably, binding of acyl-CoA substrates. It contains a bundle of 5 α-helices and a small 3_{10}-helix (α14). The orientation of these helices relative to one another is critical as judged by the number of conserved glycine residues flanking α-helical structural elements (Figure 3). In particular, glycine residues at positions 225, 241, 245, and 254 may provide the flexibility necessary for proper packing and/or formation of the α-helices. Three highly conserved aspartic acid residues are found in this domain. Asp 233 is located in the middle of helix α11, Asp 251 at the end of helix α12, and Asp 256 at the beginning of helix α13. A carboxylate oxygen from Asp 233 and Asp 251 hydrogen bonds to the hydroxyl group of Tyr 299 and Tyr 301, respectively, while Asp 256 forms a salt bridge with Lys 293. These interactions apparently stabilize the hairpin-like motif found in the C-terminal tail. This unusual secondary structure is possible due to the presence of several conserved glycine residues, Gly 291, Gly 295, and Gly 297.

The two domains are connected by a short linker region (residues 202−206) which contains a highly conserved PGF sequence (Figure 3). Figure 4 depicts residues 202−206 of this region along with the nicotinamide ring of NAD^+, residues Ser 137, His 158, and Glu 170, and several ordered water molecules. Of particular interest is the phenylalanine residue, Phe 205, which adopts a $\phi\psi$ geometry corresponding to the β-turn region of a Ramachandran plot. This unusual conformation is stabilized by numerous interactions as illustrated in Figure 4, with two ordered water molecules playing key roles. Wat 806 is coordinated to the backbone carbonyl of Phe 205 and Wat 801 to the carbonyl of Gly 204. Wat 806 is also coordinated to the hydroxyl group of Thr 202, the carbonyl of Pro 203, and another water molecule, Wat 809. Wat 801 is hydrogen bonded to Oϵ1 of Glu 170, which is also in position to coordinate Nδ1 of the active site histidine, His 158. Glu 170 provides further stabilization by positioning its Oϵ2 within hydrogen-bonding distance of the backbone amide of Ile 206. The carbonyl of Thr 202 provides the final hydrogen bond in this region through interaction with the amide of Phe 205.

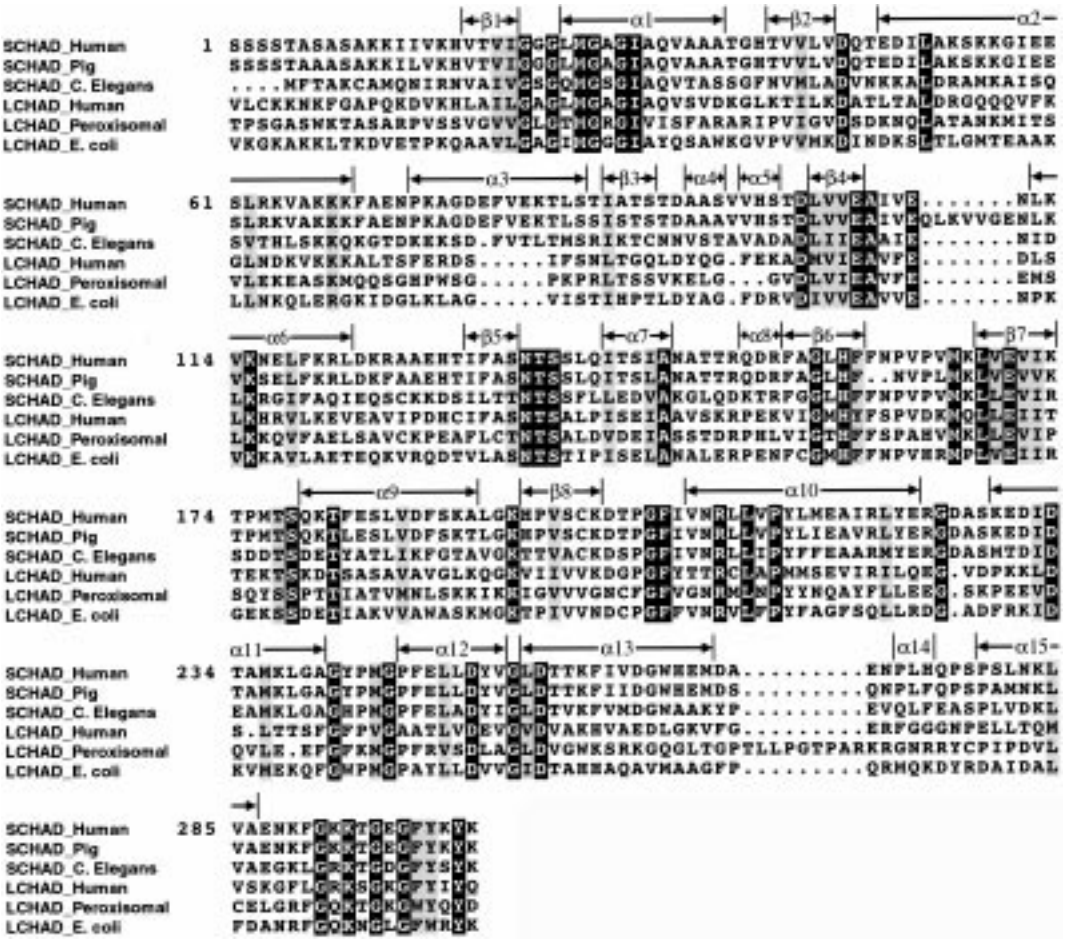

FIGURE 3: Sequence alignment of representative L-3-hydroxyacyl-CoA dehydrogenases. Perfectly conserved residues are highlighted in black and conservatively substituted residues in gray. The corresponding secondary structure for human heart SCHAD (SCHAD_Human) is indicated in brackets. Sequences used in the alignment were obtained from the Swiss-Prot database. The following labeling scheme was used, with Swiss-Prot accession numbers indicated in parentheses: SCHAD_Pig = pig heart SCHAD (P00348); SCHAD_C. Elegans = putative *Caenorhabditis elegans* SCHAD (P34439); LCHAD_Human = human mitochondrial LCHAD (P40939); LCHAD_Peroxisomal = human peroxisomal LCHAD (Q08426); LCHAD_*E. coli* = L-3-hydroxyacyl-CoA dehydrogenase of the β-oxidation complex of *Escherichia coli* (P21177).

Dimerization Interface. Subunit dimerization is mediated primarily by hydrophobic interactions between the C-terminal domains. Helix α10 (residues 207−223) of one subunit runs nearly antiparallel to helix 10 of the other subunit to form the core of the dimer interface. Helix α10 contains three highly conserved residues, Arg 209, Leu 211, and Pro 213. The side chain of Arg 209 forms a salt bridge with the carboxylate of Glu 117 on the opposing subunit to stabilize subunit dimerization. However, Glu 117 is not strictly conserved, arguing that Arg 209 may play another undefined role. Leu 211 points into the cleft between the NAD^+-binding domain and the C-terminal domain, and may play a role in substrate binding. Pro 213 is near the site of closest contact between helix 10 of each subunit at the dimer interface. However, a clear role for this conserved residue is not readily apparent.

Helix 11, corresponding to residues 229−240, makes numerous hydrophobic interactions with the final two β-strands, strands 7 and 8, of the N-terminal domain of the opposing monomer. Additional hydrophobic contacts are provided by the small helical domain, residues 273−275, of each subunit. The dimer interface is maintained by the presence of four hydrogen bonds and two salt bridges. The side chain of Asp 231 of one subunit is within hydrogen-bonding distance of the backbone amide of Ser 198 of the other subunit, as is the backbone carbonyl of Asp 226 and the main chain amide of Lys 200. As mentioned above, the side chains of Glu 217 of one subunit and Arg 209 of the other are positioned to form the two salt bridges.

Cofactor-Binding Site. The NAD^+-binding site is located at the consensus nucleotide-binding motif comprised of residues Gly22-Gly23-Gly24-Leu25-Met26-Gly27 and is adjacent to His 158, an essential active site residue (Figure 5). The quality of the electron density of the nicotinamide ring was significantly reduced compared to the rest of the cofactor in the SeMET-rSCHADH6 model, and the orientation of the pyridine ring could not be determined unambiguously. Therefore, the nicotinamide was modeled in the *syn* conformation consistent with biochemical observations of B-side specificity (*1*). As can be seen in Figure 5, the sulfur of Met 26 is in close contact with the nicotinamide ring, and initial concerns were that the disorder in this region of the cofactor was the result of the substitution of Met 26 with a larger selenomethionine residue. These concerns were confirmed upon completion of the rSCHADH6 model. Well-defined electron density for the entire cofactor was observed with the nicotinamide ring bound in the *syn* confirmation.

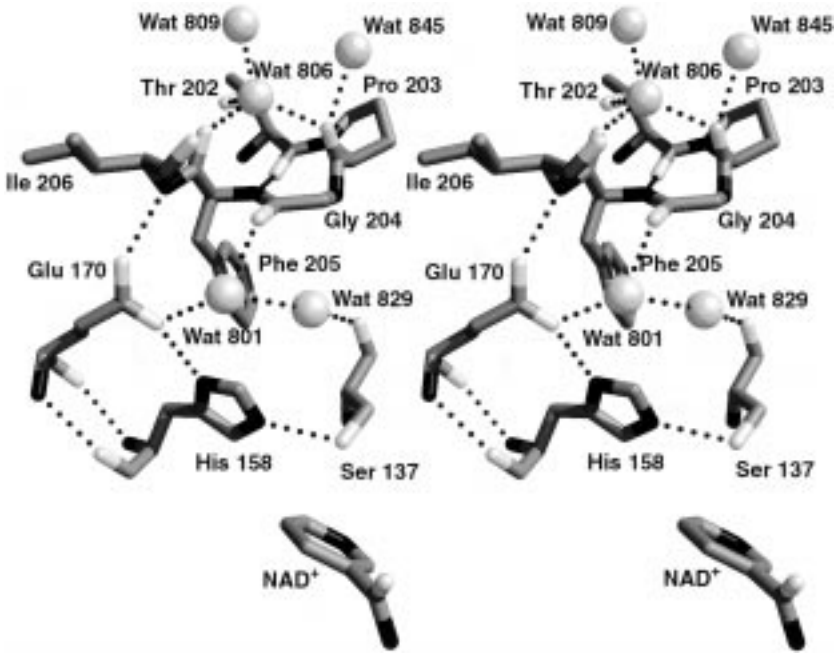

FIGURE 4: Secondary structure of the conserved PGF linker region. The stereo diagram depicts residues 202−206, which connect the NAD^+-binding domain to the C-terminal domain of the rSCHADH6 model. Oxygen atoms are colored in light gray, carbon atoms medium gray, and nitrogen atoms in black. Hydrogen bonds are illustrated as dotted black lines. The nicotinamide ring of NAD^+ is included to indicate the position of the enzyme active site. The unusual $\phi\psi$ conformation adopted by Phe 205, corresponding to the β-turn region of a Ramachandran plot, is stabilized by an intricate hydrogen bond network which includes interactions with the putative active site residues Ser 137, His 158, and Glu 170.

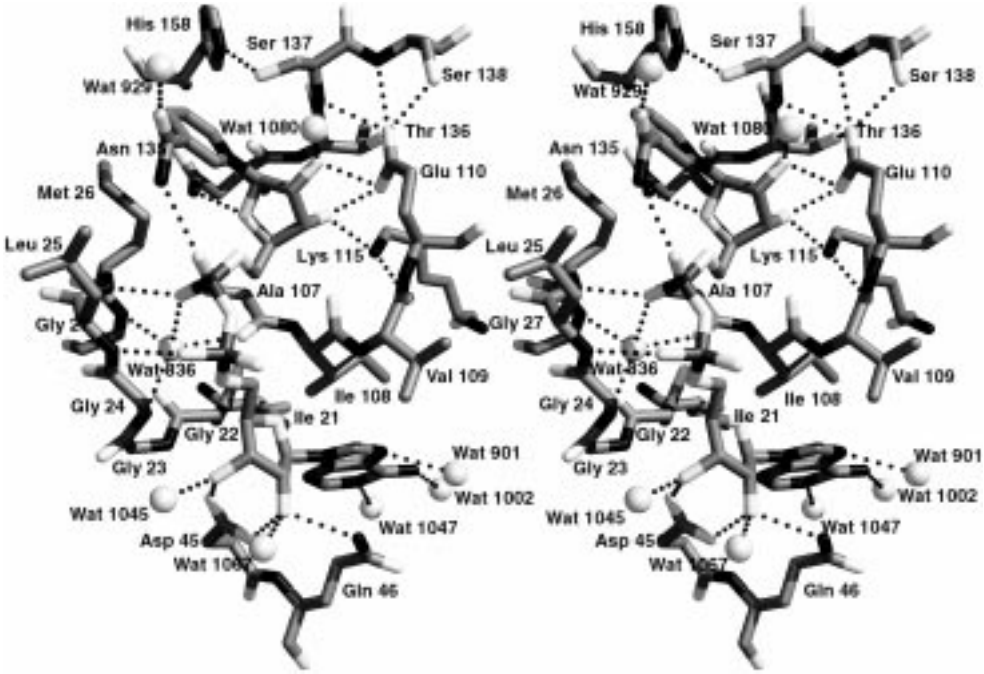

FIGURE 5: Stereo diagram of the cofactor-binding site of rSCHADH6 complexed with NAD^+. Residues of rSCHADH6 involved in the coordination of NAD^+ are illustrated, as are ordered water molecules within hydrogen bond distance of the cofactor. Hydrogen bonds are represented by dotted black lines, and atoms are colored as in Figure 4. NAD^+ is bound in an extended conformation with its nicotinamide ring (top left) in a *syn* conformation and its adenosine ring (bottom left) exposed to solvent.

Hydrogen-bonding pairs and their respective interatomic distances involved in the coordination of NAD^+ to SCHAD are listed in Table 5. The adenine portion of the cofactor is anchored in place by hydrogen bonds to its ribose hydroxyls from Asp 45 and Gln 46. Three water molecules, Wat 901, Wat 1002, and Wat 1047, are positioned to hydrogen bond with nitrogens in the adenine ring. The 2′ phosphate is coordinated by a hydrogen bond to the backbone amide of Leu 25. The bis-phosphate hydrogen bonds to the amide of Met 26 and a water molecule, Wat 836, which in turn is held by coordination to the backbone amides of Gly 24 and Gly 27, as well as to the carbonyl of Ala 107. The O4′N of the nicotinamide ribose is within hydrogen-bonding distance to Nδ2 of Asn 135. Of particular interest is the bifurcated hydrogen bond between Oϵ2 of Glu 110 and both ribose hydroxyls of nicotinamide. Glu 110 is held in position by

Table 5: Hydrogen Bond Pairs Involved in the Binding of NAD^+

hydrogen bond pair		distance (Å)
NAD:N1A[a]	Wat 1047:OH2	2.78
NAD:N6A	Wat 1002:OH2	2.85
NAD:N7A	Wat 901:OH2	2.99
NAD:O2′A	Gln 46:Nϵ2	3.05
NAD:O2′A	Asp 45:Oδ1	2.66
NAD:O2′A	Wat 1067:OH2	2.78
NAD:O3′A	Asp 45:Oδ2	2.69
NAD:O3′A	Wat 1045:OH2	2.55
NAD:O2A	Leu 25:N	2.89
NAD:O2N	Met 26:N	2.76
NAD:O2N	Wat 836:OH2	2.76
NAD:O4′N	Asn 135:Nδ2	2.95
NAD:O3′N	Glu 110:Oϵ1	2.38
NAD:O3′N	Lys 115:Nζ	2.87
NAD:O2′N	Glu 110:Oϵ1	3.07
NAD:O7N	Wat 929:OH2	2.46
NAD:N7N	NAD:O1N	3.04

[a] The atom names of NAD^+ are in accordance with current IUPAC-IUB nomenclature. Those atoms with a terminal "A" designation refer to atoms within the adenine portion of NAD^+, and similarly, those with a terminal "N" designation refer to atoms within the nicotinamide region of the molecule.

an intricate hydrogen-bonding network which includes atoms from Glu 106, Lys 115, Thr 136, and Ser 138. In addition, the hydroxyl groups of the nicotinamide ribose, O3′N and O2′N, are coordinated by Nζ of Lys 115 and a bound water, Wat 1080, respectively. Somewhat surprisingly, the nicotinamide ring does not interact with atoms from any residue except for the barrier provided by the above-mentioned Met 26. However, the nicotinamide ring may be positioned by an intramolecular hydrogen bond between the carboxamide nitrogen, N7N, and O1N, as well as by a hydrogen bond between the carboxamide oxygen, O7N, and Wat 929, which in turn hydrogen bonds to the carbonyl of Val 253. However, this water molecule is not observed in both subunits, and therefore, its significance is questionable.

Additional electron density was observed in the cavity adjacent to the nicotinamide ring. The density was large enough to contain 8−12 atoms and was continuous with several branch points. However, it was more clearly defined in the A subunit than in the B subunit. Attempts to correlate the density with components of the crystallization mother liquor or physiological substrates proved unsuccessful. The density was therefore modeled as a series of water molecules, corresponding to water numbers 959−962, 965, 966, and 1114−1116 in subunit A, for example, which refined normally.

DISCUSSION

Recombinant human heart SCHAD has been expressed in *Escherichia coli*, purified to homogeneity, and characterized using biochemical and X-ray crystallographic techniques. The dimeric enzyme exhibits a molecular weight of approximately 34 kDa/monomer and displays characteristics similar to other L-3-hydroxyacyl-CoA dehydrogenases (*4*, *6*). rSCHADH6 shows a strong preference for binding of NADH over NAD^+ as evidenced by the nearly 2 orders of magnitude difference in observed binding constants (Table 1). At pH 7.0, rSCHADH6 binds NAD^+ and NADH with dissociation constants of 85.8 ± 21.1 and 0.73 ± 0.04 μM, respectively, which are comparable to values of 120 and 0.59 μM for the rat liver enzyme (*6*). Similar trends have been observed for numerous other dehydrogenases, including alcohol, malate, and lactate dehydrogenases (*28*). rSCHADH6 functions optimally in the neutral pH range (Table 2), and the apparent V_{max} and K_m values for the conversion of acetoacetyl-CoA to L-3-hydroxybutyrl-CoA, 448 ± 7.6 μmol/min/mg and 45 ± 2.3 μM, respectively, at pH 6.0, are comparable to values obtained from the pig heart enzyme of 426 μmol/min/mg and 60 μM, respectively (*4*).

The overall fold of rSCHADH6 is comparable to a previously reported preliminary chain tracing of pig heart SCHAD at 2.8 Å resolution (*15*). The dimeric model (Figure 2) exhibits a two-domain structure with the N-terminal domain of each subunit containing an eight-stranded β-sheet. The first six β-strands are parallel and adopt a typical Rossmann fold which accommodates binding of NAD^+. The remaining two strands are also parallel but in the opposite direction of the first six. The C-terminal domain of each monomer is primarily α-helical and mediates subunit−subunit dimerization. The orientation of the NAD^+-binding domain relative to the C-terminal domain is determined by a short linker region (residues 202−206) which possesses a unique spatial arrangement (Figure 4). In addition, this unusual motif appears to be important in correct positioning of putative active site residues.

A search for homologous proteins using the program DALI (*29*) reveals, not surprisingly, considerable similarity between rSCHADH6 and numerous proteins containing a Rossmann fold, including malate and lactate dehydrogenase. However, 6-phosphogluconate dehydrogenase (6PGDH) exhibits significant structural similarity in the C-terminal domain as well, despite low sequence identity. 6PGDH is a dimeric enzyme which catalyzes the oxidative decarboxylation of 6-phosphogluconate to D-ribulose 5-phosphate with the concomitant reduction of $NADP^+$ to NADPH. It has been extensively studied using X-ray crystallography by Adams and co-workers and its catalytic mechanism well-established (*26*). The dinucleotide-binding folds of these enzymes are very similar with the major difference being the addition of the helix-turn-helix "tail" between β-strands 2 and 3 of rSCHADH6. In addition, both enzymes have a conserved methionine residue positioned adjacent to the nicotinamide ring and are "B-side"-specific dehydrogenases.

The helical domain of the 6PGDH monomer is considerably longer than the C-terminal helical domain of rSCHADH6. However, closer examination reveals a striking similarity. Adams and co-workers reported that the helical domain of 6PGDH was comprised primarily of two copies of a five-helix bundle repeat. The C-terminal domain of rSCHADH6 adopts a topology quite similar to this five-helix bundle motif, with the dimerized C-terminal domains closely resembling the complete helical domain of the 6PGDH. That is, the packing interactions which mediate dimerization of rSCHADH6 are similar to those which define the association of the two helical repeats of 6PGDH. Figure 6 depicts the two C-terminal domains of the rSCHADH6 dimer superimposed with residues 175−434 of the 6PGDH monomer. It has been suggested that the helical domain of 6PGDH was the result of a gene duplication event (*26*), and this notion is further supported by the observation of a single five-helix bundle motif in the rSCHADH6 monomer.

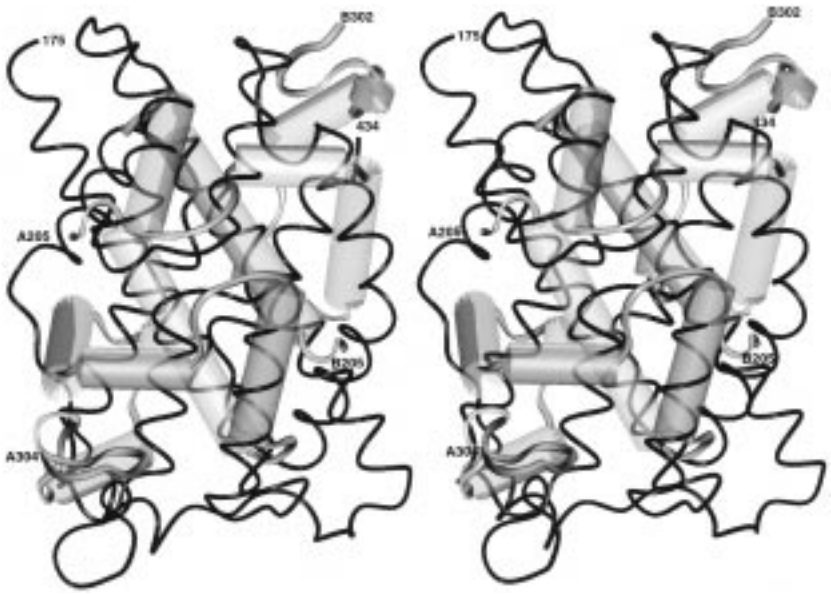

FIGURE 6: Comparison of the C-terminal domains of rSCHADH6 and 6PGDH. The dimer interface of rSCHADH6, comprised of the C-terminal domains of both subunits, is shown in gray. Helices are represented as transparent rods and linker regions as coils. The corresponding region of 6-phosphogluconate dehydrogenase, residues 175−434 of a single subunit, is depicted as a thin black ribbon in the stereo diagram.

The above-mentioned similarities between rSCHADH6 and 6PGDH strongly suggest that these two enzymes are related and that observations made in the study of 6PGDH may be applicable to SCHAD. This assumption was used to ascertain a potential L-3-hydroxyacyl-CoA binding site within rSCHADH6. The binding site of 6-phosphogluconate has been clearly identified and is located in the cleft between the N-terminal $NADP^+$-binding domain and the α-helical domain of 6PGDH. The rSCHADH6 structure was determined only in the presence of NAD^+, and therefore the L-3-hydroxyacyl-CoA site is not known. However, the equivalent contacts in rSCHADH6 would include residues in the loop connecting strands 6 and 7 of the NAD^+-binding domain, the long helix which begins the α-helical domain (helix α10), the region between helices α12 and α13, and the end of the C-terminal domain, including helix α15. To further investigate this region as the possible L-3-hydroxyacyl-CoA binding site and to identify potential residues involved in catalysis, an amino acid sequence alignment of several L-3-hydroxacyl-CoA dehydrogenases was performed and highly conserved residues were noted.

A representative amino acid sequence alignment of several L-3-hydroxacyl-CoA dehydrogenase domains is presented in Figure 3. A more comprehensive alignment using all available L-3-hydroxacyl-CoA dehydrogenase sequences was also performed (data not shown), and trends in conserved residues were maintained. Examination of the sequence alignment in the regions of the proposed L-3-hydroxacyl-CoA binding site, and more generally, the C-terminal domain, provides further insight into substrate recognition. With the exception of the conserved glycine residues, presumably required for proper folding, the remaining conserved residues in the C-terminal domain are localized in three general areas and include helix α10, the region joining helices α12 and α13, and the C-terminal tail (Figure 3). Mapping of these conserved residues in the rSCHADH6 model reveals that they are clustered near the cleft between the NAD^+-binding and C-terminal domain in the rSCHADH6 model (Figure 2), as predicted by analogy to the 6-phosphogluconate binding site of 6PGDH. Many of the side chains of these highly conserved residues are involved in hydrogen bonds with one another as described in the Results section and, therefore, are unable to participate in ligand coordination. This suggests that the overall structure in these conserved regions, and not specific side chain residues, is important in acyl-CoA substrate binding. However, the possibilty that the side chains of these conserved residues may interact with one another only in the absence of substrate cannot be discounted. Regardless, the importance of these conserved residues in acyl-CoA binding remains to be established by more than circumstantial evidence.

A prominent feature of the enzyme structure is the helix-turn-helix "tail" which connects strands β2 and β3 of the NAD^+-binding domain. This motif is similar to the large protrusion that extends from the structurally homologous FAD-binding domain of glutathione reductase (*30*), in which it is involved in subunit oligimerization. The helix-turn-helix tail of SCHAD is clearly not involved in dimerization but may serve as a handle for as yet undefined intermolecular interactions. This region is well suited for such a role, since it protrudes from the otherwise compact enzyme structure and contains numerous polar amino acid side chains whose electrostatic potentials are unfulfilled by intramolecular contacts. A sequence comparison of several L-3-hydroxyacyl-CoA dehydrogenases does not indicate strict conservation of amino acid residues in this region; however, an abundance of polar residues is clearly observed (Figure 3).

As expected, many of the highly conserved residues in the N-terminal domain are involved in cofactor binding or in specifying the overall fold of the domain. Functions of these residues have already been highlighted, but two conserved residues, His 158 and Glu 170, warrant further consideration. Recently, the importance of these two conserved residues has been studied by site-directed mutagenesis in the multienzyme complex of fatty acid oxidation from *Escherichia coli*, which contains L-3-hydroxacyl-CoA de-

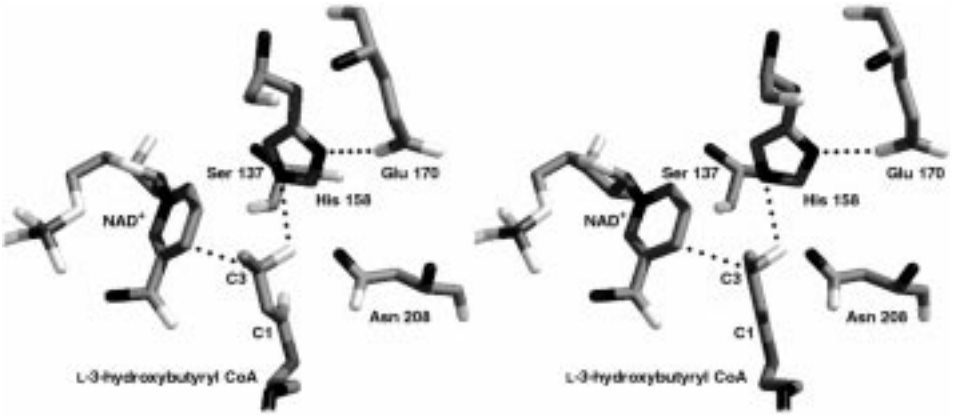

FIGURE 7: Stereo diagram of a theoretical ternary complex of L-3-hydroxybutyryl-CoA, NAD^+, and rSCHADH6. L-3-Hydroxybutyryl-CoA was modeled into rSCHADH6−NAD^+ complex using the DOCKING module of InsightII as described in Materials and Methods. Oxygen atoms are colored in light gray, carbon atoms medium gray, nitrogen atoms in black, and all others in dark gray. Interatomic interactions between the substrate, NAD^+, and the catalytic base, His 158, are represented as dotted black lines. Also depicted is the electrostatic interaction between His 158 and Glu 170. Additional residues implicated in catalysis are shown (see Discussion). However, hydrogen bonds are omitted for clarity.

hydrogenase activity (*3*, *31*). Substitution of His 450, equivalent to His 158 in SCHAD, with glutamine resulted in a 3000-fold reduction in k_{cat}. Similarly, replacement of Glu 462, equivalent to Glu 170 in SCHAD, with alanine produced a 160-fold reduction in k_{cat}. The authors suggest that His 450 serves as a general base which abstracts a proton from the L-3-hydroxyl group of the substrate and that the γ-carboxyl group of Glu 462 is involved in an electrostatic interaction with the catalytic histidine (*31*).

Examination of the crystal structure of rSCHADH6 reveals that His 158 and Glu 170 are located in the NAD^+-binding domain at the end of the sixth β-strand and in the middle of the seventh β-strand, respectively. By structural homology to 6PGDH, this region is predicted to be involved in substrate binding. These two residues are indeed within the active site, as judged by their proximity to NAD^+ (Figures 4 and 5). The Nϵ2 of His 158 is within 4.5 Å of C4 of the nicotinamide ring, the site of hydride transfer, and Oϵ1 of Glu 170 is positioned to interact with Nδ1 of His 158. Human heart SCHAD mutants, H158L and E170Q, have undetectable enzymatic activity levels, demonstrating the importance of these residues in catalysis (*2*).

Clinically, the requirement of a glutamic acid residue within the active site of human long chain L-3-hydroxyacyl-CoA dehydrogenase (LCHAD) has been demonstrated. Maternal acute fatty liver of pregnancy (AFLP) is a late term gestational complication that results in significant maternal and fetus morbidity and mortality. Occurrence of AFLP has been correlated to the presence within the fetus of either homozygous or compound heterozygous mutations in the α-subunit of the mitochondrial trifunctional protein (*14*, *32*). Specifically, the E474Q mutation is the determinant for the disease state. Glu 474 is equivalent to Glu 170 in human heart SCHAD, and as can be seen in Figure 5, a substitution with glutamine would disrupt the electrostatic interaction between Oϵ1 of Glu 170 and Nδ1 of His 158, which is thought to be essential for catalysis. In addition, this mutation may be disruptive to the contacts within the conserved PGF region which relates the positions of the two domains of the protein. It has been demonstrated that an E462Q mutation in the multienzyme complex of fatty acid oxidation from *Escherichia coli*, equivalent to an E474Q mutation in human trifunctional protein, greatly reduces the thermostability of the enzyme complex (*31*).

To develop a comprehensive model of catalysis by rSCHADH6, molecular modeling studies were conducted. L-3-Hydroxybutyryl-CoA was modeled into the active site of rSCHADH6 based on similarities to 6PGDH and the localization of conserved residues within the C-terminal domain. In this fashion, the acyl chain was positioned at the interface of the NAD^+-binding domain and the C-terminal domain, and the coenzyme A component of the substrate was placed along the conserved residues adjacent to the active site cleft. Furthermore, the orientation of L-3-hydroxybutyryl-CoA was set such that the carbon at position 3 would be adjacent to C4 of the nicotinamide ring and the L-3-hydroxyl group of the substrate would be within hydrogen bond distance of Nϵ2 of His 158 (Figure 7) as suggested by mutagenesis studies (*2*, *3*). This arrangement suggests that two other highly conserved residues, Ser 137 and Asn 208, may be important in catalysis based on their proximity to the modeled L-3-hydroxyacyl-CoA substrate. However, it is important to note that significant conformational changes that are difficult to predict by molecular modeling studies may occur upon binding the acyl-CoA substrate. In fact, attempts to generate an abortive ternary complex for crystallographic studies by soaking acetoacetyl-CoA into crystals of rSCHADH6 complexed with NAD^+ have been unsuccessful due to crystal cracking, suggesting possible minor conformational rearrangements. Efforts are currently underway to co-crystallize an abortive ternary complex.

In the current model of rSCHADH6 complexed with NAD^+, Ser 137 is within hydrogen-bonding distance of Nϵ2 of His 158, and Asn 208 is pointed into the putative active site. The arrangement of Glu 170, His 158, and Ser 137 is reminiscent of the classic catalytic triad found in serine proteases. However, in the context of the dehydrogenase reaction catalyzed by the enzyme, an activated serine residue capable of nucleophilic attack does not appear relevant. More likely, Ser 137 is fulfilling a more pedestrian role. For example, the hydroxyl group of Ser 137 may help facilitate hydride transfer by stabilizing the localized positive charge which develops at C4 of the nicotinamide ring of NAD^+ during catalysis. Such a role has been proposed for Thr 246

of *Bacillus stearothermophilus* L-lactate dehydrogenase (*33*). Alternatively, modeling studies with L-3-hydroxybutyryl-CoA indicate that the side chain of Ser 137 may interact with the negative charge that develops on O3 of the hydroxyl substrate during the transition state. A similar role for the side chain amide of Asn 208 is also suggested (Figure 7). Recent studies of malate dehydrogenase indicate that the side chains of Arg 87 and Asn 119 serve such a function during conversion of malate to oxaloacetate (*34*). In addition, the side chain amide of Asn 208 is within hydrogen-bonding distance of the C1 carbonyl oxygen of the substrate. Such an interaction could facilitate catalysis by lowering the pK_a of the C3 hydroxyl group. Finally, Ser 137 and Asn 208 may simply be involved in substrate coordination and/or structural arrangement of the active site. Clearly, the aforementioned roles are speculative and require further study.

The above observations cumulatively suggest a possible model for catalysis by human heart SCHAD. Binding of the L-3-hydroxyl-CoA substrate occurs at the interface of the NAD^+-binding domain and the C-terminal domain. His 158 serves as a general base by abstracting a proton from the L-3-hydroxyl group of the substrate. The subsequent ketonization of the C3−O bond facilitates the hydride transfer from C3 of the substrate to C4 of the nicotinamide ring (Figure 7). This model specifies an initial proton abstraction, but a concerted mechanism or a mechanism in which hydride transfer occurs prior to proton abstraction cannot be excluded. Furthermore, several aspects of catalysis require clarification. In addition to the possible roles of Ser 137 and Asn 208 mentioned above, the importance of the electrostatic interaction between the active site histidine, His 158, and Glu 170 is particularly intriguing. Intuitively, such an interaction might serve to elevate the pK_a of the histidine residue. However, mutagenesis studies in which the glutamate residue of an analogous active site pair has been replaced by a glutamine residue suggest that glutamate does not affect the pK_a of histidine (*31*), arguing against such a role.

In summary, human heart SCHAD has been characterized by biochemical and crystallographic techniques. The enzyme structure is comprised of two domains, the NAD^+-binding domain and the helical C-terminal domain. Catalysis is thought to occur in the cleft between these domains by a mechanism similar to other dehydrogenases. In particular, an active site histidine, His 158, serves as a general base in the proton abstraction step in the biologically relevant forward reaction. The ability of this histidine to perform such a function is enhanced through an electrostatic interaction with an acidic residue, Glu 170. Other residues that may serve a role in catalysis are suggested by examination of the active site structure. Future biochemical and mutagenesis studies of the protein will be assisted by scrutiny of the crystal structure and will continue to provide insights into human disease states.

ACKNOWLEDGMENT

The authors recognize Ed Hoeffner for his contributions through the maintenance of the X-ray and computational resources at the University of Minnesota and also Axel Brünger for providing us with the beta version of CNS. The authors acknowledge the valuable contributions of Gerd Rosenbaum and Ed Westbrook in the design and construction of the 19-ID beamline at Argonne National Laboratory and Andrezj Joachimiak and the rest of the SBC staff for their efforts in the final testing and commissioning of the beamline. We thank Nancy Raha and Dr. Leo Bonilla of the Mass Spectrometry Facility at the University of Minnesota Cancer Center for enzyme mass determinations. Finally, we acknowledge Dr. Colin Thorpe (University of Delaware) and Dr. Melanie Simpson for thoughtful discussions regarding the manuscript.

REFERENCES

1. Noyes, B. E., Glatthaar, B. E., Garavelli, J. S., and Bradshaw, R. A. (1974) *Proc. Natl. Acad. Sci. U.S.A. 71*, 1334−1338.
2. O'Brien, L. K., Sims, H. F., Gibson, B., and Strauss, A. W. (1998) submitted for publication.
3. He, X. Y., and Yang, S. Y. (1996) *Biochemistry 35*, 9625−9630.
4. Noyes, B. E., and Bradshaw, R. A. (1973) *J. Biol. Chem. 248*, 3052−3059.
5. El-Fakhri, M., and Middleton, B. (1982) *Biochim. Biophys. Acta 713*, 270−279.
6. Osumi, T., and Hashimoto, T. (1980) *Arch. Biochem. Biophys. 203*, 372−383.
7. Novikov, D. K., Vanhove, G. F., Carchon, H., Asselberghs, S., Eyssen, H. J., Van Veldhoven, P. P., and Mannaerts, G. P. (1994) *J. Biol. Chem. 269*, 27125−27135.
8. Mulders, J. W. M., Hendriks, W., Blackesteijn, M., Bloemendal, H., and de Jong, W. W. (1988) *J. Biol. Chem. 263*, 15462−15466.
9. Roe, C. R., and Coates, P. M. (1995) in *The Metabolic and Molecular Bases of Inherited Disease* (Scriver, C. R., Beaudet, A. L., Sly, W. E., and Valle, D., Eds.) 7th ed., pp 1501−1533, McGraw-Hill, New York, NY.
10. Schulz, H. (1996) in *Biochemistry of Lipids, Lipoproteins and Membranes* (Vance, D. E., and Vance, J., Eds.) pp 75−99, Elsevier, Amsterdam.
11. Furuta, S., Kobayashi, A., Miyazawa, S., and Hashimoto, T. (1997) *Biochim. Biophys. Acta 1350*, 317−324.
12. Bennett, M. J., Weinberger, M. J., Kobori, J. A., Rinaldo, P., and Burlina, A. B. (1996) *Pediatr. Res. 39*, 185−188.
13. Pons, R., Roig, M., Riudor, E., Ribes, A., Briones, P., Ortigosa, L., Baldellou, A., Gil-Gibernau, J., Olesti, M., Navarro, C., and Wanders, R. J. A. (1996) *Pediatr. Neurol. 14*, 236−243.
14. Isaacs, J. D., Jr., Sims, H. F., Powell, C. K., Bennett, M. J., Hale, D. E., Treem, W. R., and Strauss, A. W. (1996) *Pediatr. Res. 40*, 393−398.
15. Birktoft, J. J., Holden, H. M., Hamlin, R., Xuong, N. H., and Banaszak, L. J. (1987) *Proc. Natl. Acad. Sci. U.S.A. 84*, 8262−8266.
16. Vredendaal, P. J. C. M., van den Berg, I. E. T., Malingre, H. E. M., Stroobants, A. K., OldeWeghuis, D. E. M., and Berger, R. (1996) *Biochem. Biophys. Res. Commun. 223*, 718−23.
17. Ramakrishnan, V., Finch, J. T., Graziano, V., Lee, P. L., and Sweet, R. M. (1993) *Nature 362*, 219−223.
18. Rodgers, D. W. (1997) *Methods Enzymol. 276*, 183−203.
19. Hendrickson, W. A. (1991) *Science 254*, 51−58.
20. Otwinowski, Z., and Minor, W. (1997) *Methods Enzymol. 276*, 307−326.
21. Terwilliger, T. C., and Berendzen, J. (1997) *Acta Crystallogr. D53*, 571−579.
22. Levitt, D. G., and Banaszak, L. J. (1993) *J. Appl. Crystallogr. 26*, 736−745.
23. Brünger, A. T., Adams, P. D., Clore, G. M., DeLano, W. L., Gros, P., Grosse-Kunstleve, R. W., Jiang, J., Kuszewski, J., Nilges, M., Pannu, N. S., Read, R. J., Rice, L. M., Simonson, T., and Warren, G. L. (1998) *Acta Crystallogr. D54*, 905−921.
24. Jones, T. A., Zou, J. Y., Cowan, S. W., and Kjeldgaard, M. (1991) *Acta Crystallogr. A47*, 110−119.
25. Engel, C. K., Mathieu, M., Zeelan, J. P., Hiltunen, J. K., and Wierenga, R. K. (1996) *EMBO J. 15*, 5135−5145.

26. Adams, M. J., Ellis, G. H., Gover, S., Naylor, C. E., and Philips, C. (1994) *Structure 2*, 651−668.
27. Laskowski, R. A., MacArthur, M. W., Moss, D. S., and Thornton, J. M. (1993) *J. Appl. Crystallogr. 26*, 283−291.
28. Dalziel, K. (1975) in *The Enzymes* (Boyer, P. D., Ed.) pp 2−61, Academic Press, Inc., New York, NY.
29. Holm, L., and Sander, C. (1993) *J. Mol. Biol. 233*, 123−138.
30. Mittl, P. R. E., and Schulz, G. E. (1994) *Protein Sci. 3*, 799−809.
31. He, X. Y., Deng, H., and Yang, S. Y. (1997) *Biochemistry 36*, 261−268.
32. Ibdahl, J. A., Bennett, M. J., Rinaldo, P., Zhao, Y., Gibson, B., Sims, H., and Strauss, A. W. (1998) submitted for publication.
33. Sakowicz, R., Kallwass, H. K. W., Parris, W., Kay, C. M., Jones, J. B., and Gold, M. (1993) *Biochemistry 32*, 12730−12735.
34. Cunningham, M. A., Ho, L. L., Nguyen, D. T., Gillilan, R. E., and Bash, P. A. (1997) *Biochemistry 36*, 4800−4816.

BI9829027